Published online 18 August 2006 *Nucleic Acids Research, 2006, Vol. 34, No. 15* ***4269–4277***
doi:10.1093/nar/gkl567

Structural basis for topoisomerase VI inhibition by the anti-Hsp90 drug radicicol

Kevin D. Corbett and James M. Berger*

Department of Molecular and Cellular Biology, 237 Hildebrand Hall #3206, University of California, Berkeley, Berkeley, CA 94720-3206, USA

Received June 22, 2006; Revised and Accepted July 21, 2006

ABSTRACT

Members of the GHL ATPase superfamily, including type II topoisomerases, Hsp90-class chaperones, and MutL, all share a common GHKL-type ATP-binding fold and act as nucleotide-controlled 'molecular clamps'. These enzymes' ATP-binding sites have proven to be rich drug targets, and certain inhibitors of type II topoisomerases and Hsp90 bind to this region and competitively inhibit these enzymes. Recently, it was found that radicicol, a drug known to block Hsp90 function, also inhibits the archaeal type IIB topoisomerase topo VI. Here, we use X-ray crystallography to show that despite low sequence identity (~10–12%) between topo VI and Hsp90, radicicol binds to the ATPase sites of these two enzymes in an equivalent manner. We further demonstrate that radicicol inhibits both the dimerization of the topo VI ATPase domains and ATP hydrolysis, two critical steps in the enzyme's strand passage reaction. This work contributes to a growing set of structures detailing the interactions between GHL-family proteins and various drugs, and reveals radicicol as a versatile scaffold for targeting distantly related GHL enzymes.

INTRODUCTION

Type II topoisomerases are essential enzymes that maintain the structural and topological integrity of cellular DNA. These enzymes are unique in their ability to pass one DNA duplex through a transient double-stranded break in another, a reaction controlled by the binding and hydrolysis of two molecules of ATP (1–3). Through this activity, type II topoisomerases can resolve a variety of potentially dangerous DNA topologies, including supercoils, knots and catenanes (4). Additionally, because cells need to appropriately maintain DNA superstructure for growth and division, many compounds that target type II topoisomerases exhibit useful therapeutic properties (5–7).

The duplex passage reaction of type II topoisomerases [reviewed in Ref. (3)] begins when the enzyme binds one segment of DNA, known as the 'gate' or G-segment (8). A second DNA, the 'transfer' or T-segment, is next trapped inside the enzyme upon ATP-induced dimerization of the nucleotide-binding domains (9,10). ATP binding and T-segment capture in turn stimulate attack of the G-segment by a pair of tyrosine residues, creating a reversible double-stranded DNA break. A series of conformational changes, likely facilitated by ATP hydrolysis, are subsequently propagated through the enzyme to separate the two broken G-segment ends, transport the T-segment though the break, and expel the T-segment from the enzyme (8). Following ATP hydrolysis and product release, the ATPase domains dissociate, resetting the enzyme for another round of strand passage (10,11).

Type II topoisomerases (topos) are divided into two groups that share a common set of catalytic domains but are structurally and evolutionarily distinct. The type IIA enzymes, including bacterial DNA gyrase and topo IV, eukaryotic topo II and phage type II topos, were discovered over 30 years ago (12), and have been extensively studied both biochemically and structurally [for reviews, see Refs. (1–4)]. In contrast, relatively less is known about topo VI, a type IIB enzyme first isolated by Forterre and colleagues (13) that has been found throughout archaea as well as in algae, plants and a small number of bacteria (13–16). The ATPase domains of topo VI are similar to those of its type IIA cousins (14,17), but topo VI possesses a distinct DNA-binding and cleavage subunit that is homologous to the meiotic recombination factor Spo11 (14,18,19). Interestingly, despite the differences between the DNA cleavage domains of the type IIA and IIB topoisomerases, several drugs that affect G-segment cleavage in eukaryotic enzymes (e.g. doxorubicin/donorubicin and amsacrines) have been shown to also inhibit topo VI (13). In contrast, drugs such as the coumarins, which target the ATPase regions of bacterial type IIA topoisomerases, do not appear to cross-react with type IIB enzymes (13).

The ATPase domains of all type II topoisomerases adopt a GHKL fold, named for the founding members of this class: DNA gyrase, Hsp90, bacterial histidine kinases and MutL (14,20). Three of these enzyme families, including type II

*To whom correspondence should be addressed. Tel: +1 510 643 9483; Fax: +1 510 643 9290; Email: jmberger@berkeley.edu

topoisomerases, Hsp90 and MutL, form the 'GHL' sub-class that possesses an additional domain and some common mechanistic features (10,17,21). Despite their widely diverse cellular functions, GHL enzymes are all 'molecular clamps': type II topos and MutL trap substrates through ATP-dependent dimerization of these domains (9,10,22), while Hsp90 seems to use GHKL domain dimerization to facilitate the release of bound substrates (23).

The evolutionary kinship between the ATPase domains of different GHL enzymes recently prompted Forterre and co-workers to test the ability of two Hsp90 inhibitors, geldanamycin and radicicol, to inhibit type II topoisomerases (24). While neither drug inhibited the bacterial type IIA topoisomerase, DNA gyrase, radicicol was shown to effectively inhibit strand passage by the archaeal type IIB enzyme topo VI. This finding was remarkable, especially in light of the very low sequence identity (10–12% identity) and structural homology (6.5 Å Cα r.m.s.d.) that exists between the GHKL domains of topo VI and Hsp90. Based on radicicol's ability to inhibit topo VI and on molecular modeling studies, Gadelle *et al*. (24) proposed that radicicol likely acts on this enzyme as it does on Hsp90, by binding to the ATPase site.

Here we show through crystallographic analyses that radicicol inhibits topo VI by associating with the enzyme's ATP-binding pocket in a manner that closely mimics its interaction with Hsp90. In addition, we show that radicicol behaves similarly to competitive ATPase inhibitors of bacterial type IIA topoisomerases, such as novobiocin (25), and that it can effectively block nucleotide-mediated dimerization of the topo VI ATPase subunit. These results provide important mechanistic insights into the mode of action of the first drug identified to inhibit topo VI via its ATPase subunit, and help further define the interplay between drug structure and enzyme specificity for GHL-family proteins.

MATERIALS AND METHODS

Cross-linking based dimerization assay

A near full-length fragment containing residues 2–470 of the *Sulfolobus shibatae* topoisomerase VI B-subunit (topoVI-B′) was prepared as described previously (17). Purified topoVI-B′ was diluted to 2 mg/ml in a buffer containing 20 mM HEPES (pH 7.5), 400 mM NaCl, 10% glycerol and 1% dimethyl sulfoxide (DMSO) (from radicicol stock solution), along with 1 mM of either ADP, AMP-PNP or radicicol (Sigma). When both nucleotide and radicicol were included, the protein was pre-incubated with 1 mM radicicol at room temperature for 30 min before nucleotide addition. Reactions were incubated at 65°C for 10 min and slow-cooled (1°C/min) to room temperature in a hot-top thermocycler to minimize evaporation (dimerization was not observed without a high-temperature incubation, presumably because of the thermophilic nature of the enzyme). Samples were then diluted 8-fold in buffer and fresh glutaraldehyde was added to 0.025%. After 20 min, 10 µl aliquots were removed and quenched with 5 µl 2 M glycine. Finally, 10 µl SDS–PAGE loading dye was added and 15 µl of each sample was run on an 8% SDS–polyacrylamide gel.

ATPase assay

ATPase assays were performed using a modified malachite green/molybdate assay for free phosphate as described previously, with adjustments to reduce sample volume and increase assay sensitivity (26,27). Reactions (25 µl) contained 10 µM topoVI-B′, 1 mM ATP and varying amounts of radicicol (20 µM to 1 mM) in a buffer composed of 20 mM HEPES (pH 7.5), 300 mM NaCl, 5% glycerol, 1 mM DTT and 1% DMSO (from radicicol stock solution). Reactions were initiated with the addition of enzyme and incubated for 20 min at 75°C in a hot-top thermocycler. After incubation, 64.5 µl of assay reagent [two parts 0.0675% (w/v) malachite green in water, one part 5% (w/v) ammonium molybdate tetrahydrate in 4 M sulfuric acid, mixed and filtered the day of the assay] was added to each reaction. After 1 min, 10.5 µl of 34% (w/v) sodium citrate in water was added to quench the reaction and minimize acid hydrolysis of remaining ATP. Color was allowed to develop for 30 min, and a Perkin-Elmer Victor3V plate reader recorded absorbance with an excitation filter at 665 nm (7.5 nm bandpass). All reactions were performed in triplicate.

Crystallization, data collection and structure solution

For co-crystallization trials, topoVI-B′ (10–15 mg/ml) was dialyzed overnight against 20 mM HEPES (pH 7.5), 100 mM NaCl and 5 mM $MgCl_2$. After dialysis, radicicol was added to 1 mM (from a 100 mM stock in DMSO), and the mixture was incubated at room temperature for 30 min before setting crystal trays.

Crystallization was performed in microbatch format under paraffin oil. Dialyzed topoVI-B′ was mixed 1:1 with well solution containing 250 mM magnesium acetate, 24% PEG-3350 and 100 mM HEPES (pH 7.5) at 19°C. Following crystallization, the drop was flooded with cryoprotectant containing an additional 25% glycerol, and crystals (flat plates $\sim 0.4 \times 0.4 \times 0.02$ mm) were looped and flash-frozen in liquid nitrogen.

All datasets were collected on Beamline 8.3.1 at the Advanced Light Source at Lawrence Berkeley National Laboratory (28). Diffraction data were indexed and reduced with ELVES (29) using MOSFLM (30). Molecular replacement was performed with PHASER (31), using the previously reported monomeric apo structure of topoVI-B′ (PDB ID 1MU5) (17) as a search model. To avoid biasing the refinement process, we used a free-R set identical to that used in the original refinement of the search model. Refinement and placement of ordered water molecules was carried out using a Refmac/ARP procedure (32,33), followed by TLS refinement as implemented in Refmac5 (34). The final model contains residues 10–470 of topoVI-B′, with 98.7% of residues in favored regions and no residues in disallowed regions of Ramachandran space. $F_o - F_c$ simulated-annealing omit maps were generated by CNS (35,36). Buried surface area was computed with AREAIMOL (37), and surface complementarity by SC (37,38). Figures were produced with PyMOL (39). Coordinates have been deposited in the RCSB PDB under accession no. 2HKJ.

RESULTS AND DISCUSSION

Radicicol inhibits ATP hydrolysis and nucleotide-mediated dimerization of topo VI-B′

We have described previously the purification and crystallization of the isolated 470 amino acid ATPase region of the *S.shibatae* topo VI B-subunit (topoVI-B′) (17). This construct consists of the GHKL ATP-binding domain, as well as a C-terminal 'transducer' domain that is involved in nucleotide turnover and likely acts to sense and respond to ATP- and/or T-segment binding (10,11). These domains are separated by a small helix-two turns-helix (H2TH) domain of unknown function, which is not shared with other type II topos or Hsp90. The C-terminal 60 amino acids of topoVI-B, responsible for interaction with the A-subunit (17), are truncated in the topoVI-B′ construct.

To test whether radicicol acts on topo VI through the enzyme's ATPase domains, we first measured the drug's effect on ATP hydrolysis by the topoVI-B′ construct. Figure 1A shows that radicicol significantly impairs the ATPase activity of topoVI-B′ at concentrations equivalent to those in which it has been shown to inhibit strand passage (24). These data indicate that the nucleotide-binding site of topo VI comprises the site of radicicol action.

Since dimerization of the ATPase domains is also dependent on ATP-binding, we next sought directly to determine the effect of radicicol on the dimerization of topoVI-B′. If the drug were to interact directly with the ATP-binding site of topo VI, it could impair strand passage either by inhibiting dimerization of the GHKL domains, or by 'locking' them in a dimeric state that is impaired in its ability to release hydrolysis products. Precedent for both of these mechanisms can be found in different drugs that target type IIA topoisomerases. For example, bisdioxopiperazines bind between the dimerized GHKL domains of eukaryotic topo II and hold this interface closed (40,41). In contrast, novobiocin inhibits bacterial type IIA topoisomerases by impeding ATP binding and GHKL domain dimerization (25,42). Since radicicol was expected to bind directly to the ATP-binding pocket of topoVI-B′ (24), we anticipated that its activity would more closely mimic that of novobiocin.

To test this assumption, we made use of a dimerization assay for topoVI-B′ based on glutaraldehyde cross-linking (11). We have shown previously that topoVI-B′ is monomeric in solution in the absence of nucleotide, and that ATP or a non-hydrolyzable analog is able to induce measurable amounts of dimerization (11). As shown in Figure 1B, radicicol on its own does not promote dimerization of topoVI-B′. The drug also effectively inhibits nucleotide-dependent dimerization when pre-incubated with the protein. Together with the results of our ATPase assays, these data support the idea that radicicol inhibits topo VI by binding to the ATPase site of the enzyme's B-subunit, preventing both ATP binding and GHKL domain homo-dimerization.

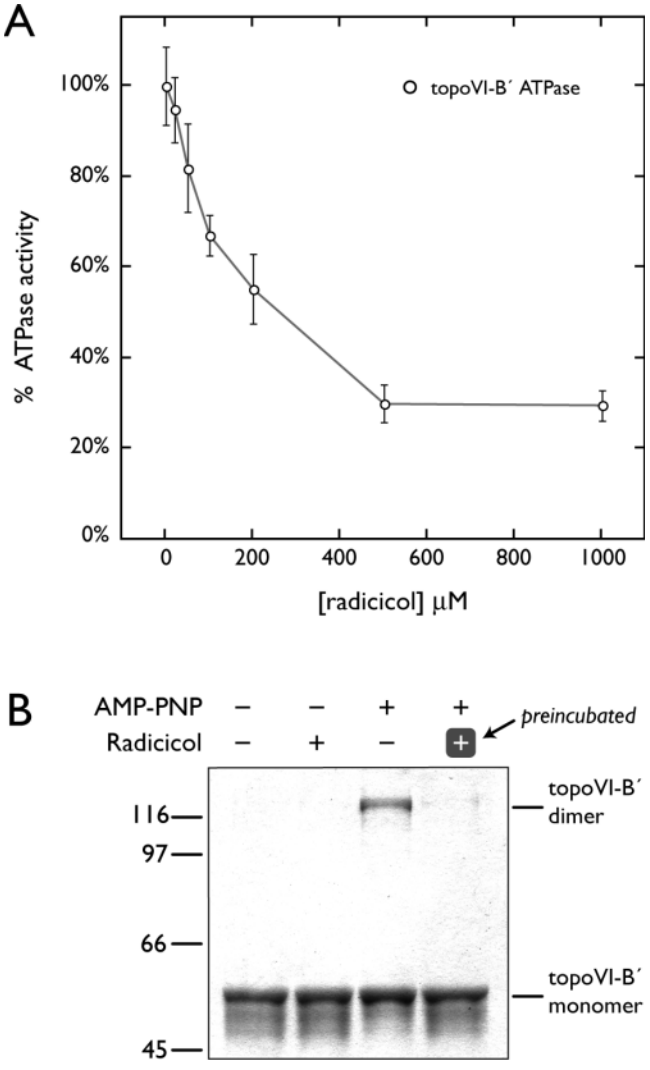

Figure 1. The effect of radicicol on ATP turnover and nucleotide-induced dimerization of topoVI-B′. (**A**) Radicicol inhibits ATP hydrolysis by topoVI-B′. Since the intrinsic ATPase activity of the isolated topoVI-B′ subunit is very low (~0.11 ATP hydrolyzed per minute per subunit), the observed residual activity may be attributable to a contaminating ATPase activity i.e. radicicol-resistant. Error bars indicate the standard deviation between three trials conducted in parallel. (**B**) Radicicol blocks dimerization of topoVI-B′. Glutaraldehyde based cross-linking dimerization assay, performed in the presence and absence of radicicol and the non-hydrolyzable ATP analog, AMP-PNP. Radicicol does not stimulate dimerization on its own (lane 2), and significantly inhibits dimerization mediated by AMP-PNP when pre-incubated with the protein (lane 4). For this assay, the drug was pre-incubated with topoVI-B′ to avoid detecting any dimers that may form before equilibrium is reached, since AMP-PNP-mediated dimerization is essentially irreversible.

The structure of topoVI-B′ bound to radicicol

Since radicicol effectively inhibits topo VI strand passage activity (24), ATP turnover, and nucleotide-dependent GHKL domain dimerization, we next set out to directly visualize the drug's binding to topoVI-B′. We attempted to crystallize a topoVI-B′–radicicol complex in conditions matching those previously reported for either dimeric or monomeric forms of the protein (17). In accord with the results of our dimerization assay, we were only able to grow crystals of the complex in the monomeric state. Using diffraction data collected from these crystals, we solved the structure by molecular replacement to a resolution of 2.0 Å (Table 1).

The structure of the topoVI-B′–radicicol complex is shown in Figure 2. The drug binds to the topoVI-B′ GHKL domain

Table 1. Data collection, refinement and stereochemistry

Data collection	
Resolution (Å)	50–2.0
Wavelength (Å)	1.1157
Space group	$P2_12_12$
Unit cell dimensions (a, b, c) Å	93.88, 111.40, 54.89
Unit cell angles (α, β, γ)°	90.0, 90.0, 90.0
I/σ (last shell)	10.5 (2.2)
R_{sym} (last shell) %[a]	6.4 (32.2)
Completeness (last shell) %	99.0 (94.6)
No. of reflections	143 571
Unique	39 306
Refinement	
Resolution (Å)	30.0–2.0
No. of reflections	35 959
Working	32 723
Free (% total)	3236 (8.3%)
R_{work} (last shell) (%)[b]	16.67 (22.4)
R_{free} (last shell) (%)[b]	20.88 (27.2)
Structure and Stereochemistry	
No. of atoms	4089
Protein	3704
Water	355
Radicicol	25
Magnesium	1
DMSO	4
R.m.s.d. bond lengths (Å)	0.015
R.m.s.d. bond angles (°)	1.410

[a]$R_{sym} = \Sigma\Sigma_j|I_j - \langle I\rangle|/\Sigma I_j$, where I_j is the intensity measurement for reflection j and $\langle I\rangle$ is the mean intensity for multiply recorded reflections.
[b]$R_{work,\ free} = \Sigma||F_{obs}| - |F_{calc}||/|F_{obs}|$, where the working and free *R*-factors are calculated using the working and free reflection sets, respectively. The free reflections were held aside throughout refinement.

in much the same manner as it does to Hsp90, with the aromatic ring binding in the interior of the ATP-binding pocket and the macrocycle draping over the outer edge of the pocket. Radicicol interacts with topoVI-B′ through several water-mediated hydrogen bonds, two direct hydrogen bonds between exocyclic oxygen atoms of the aromatic ring and the side chains of Asp76 and Thr170, and van der Waals interactions between the exocyclic chlorine atom and the side chains of Val112 and Phe90. In addition to these specific contacts, there are several van der Waals contacts between the macrocycle ring and surrounding hydrophobic residues, resulting in excellent overall shape complementarity between the drug and its binding site (Figure 2 and Table 2).

Comparison of radicicol- and AMP-PNP-bound forms of topoVI-B′ shows that the drug binding site directly overlaps with that of the nucleotide (Figure 3A and B). Further inspection also reveals why the drug is unable to mediate dimerization of the subunit. When AMP-PNP (a non-hydrolyzable ATP analog) binds to the GHKL domain of topoVI-B′, the ATP lid (residues 107–111) drapes across the γ-phosphate moiety, and an adjacent loop (residues 97–106) rearranges to interact directly with the ribose and β-phosphate groups of the nucleotide. These structural changes in turn allow ~10 residues from the extreme N-terminus of the dimer mate (a region termed the 'strap') to drape across this loop and effectively lock the dimer together (10,11). In contrast, radicicol binding does not induce the rearrangement of either the ATP lid or the adjacent loop. Indeed, the drug may actively inhibit these changes, as it lacks similarity to adenine in both shape and chemical nature (Figure 3B), and appears unable to support hydrogen bonding interactions needed for the conformational rearrangements that accompany binding of the N-terminal strap.

Comparison of radicicol binding to other drugs targeting type II topoisomerase ATPase domains

Type II topoisomerases from bacteria, archaea and eukaryotes all share a common set of ATPase domains (10,17,40). Thus, it is noteworthy that, of the several classes of drugs that inhibit type II topoisomerases by targeting their ATPase domains, most act on only a subset of family members. Fortunately, complexes between several of these drugs and their respective targets have been amenable to analysis by X-ray crystallography, allowing a detailed comparison of their modes of action and unique specificity determinants (43).

One class of drugs, the bisdioxopiperazines, associates with the GHKL domains of eukaryotic type II topoisomerases and inhibits the enzyme non-competitively (44). Bisdioxopiperazines have been shown to act by binding in a cavity between dimer-related GHKL domains, effectively locking these two subunits together to prevent the enzyme from turning over (40). The bisdioxopiperazines specifically target eukaryotic type IIA topoisomerases because the cavity in which they bind is not conserved in the bacterial type IIA or archaeal type IIB topos (40). This mode of action is distinctly different from that of radicicol, which blocks dimerization of the GHKL domains of topo VI (Figure 1B).

A more informative study can be undertaken by comparing the action of radicicol with that of compounds targeting bacterial type IIA topoisomerases, in particular DNA gyrase. Complexes between the *Escherichia coli* GyrB subunit and coumarin drugs (novobiocin and chlorobiocin), as well as a peptide-based cyclothialidine analog (GR122222X), have been studied crystallographically, and show that both of these drug classes inhibit strand passage by competitively binding to the ATPase site (25,45,46). In this respect, the action of these drugs parallels that of radicicol. Moreover, overlays of co-crystal structures indicate that these drugs' binding sites overlap with the adenine of bound nucleotide, as is seen for radicicol, and that the compounds likewise possess no structural analog to the ribose sugar or phosphate moieties (Figure 3C and D).

Despite these similarities, a comparison of the radicicol-binding site in topoVI-B′ with that seen for novobiocin and GR122222X in *E.coli* GyrB reveals the structural basis for these compounds' distinct specificities. All three drugs interact with two highly conserved residues, $Asp76^{topoVI\text{-}B'}$/$Asp73^{GyrB}$ and $Thr170^{topoVI\text{-}B'}$/$Thr165^{GyrB}$, which directly contact ATP in all type II topoisomerases. Radicicol and GR122222X are also liganded by the main chain nitrogen of $Gly80^{topoVI\text{-}B'}$/$Gly77^{GyrB}$ and the main chain carbonyl oxygen of $Leu39^{topoVI\text{-}B'}$/$Val43^{GyrB}$, residues that ligand either ATP or Mg^{2+} in both topoVI-B′ and GyrB. However, novobiocin and GR122222X further interact with another conserved residue, $Asn42^{topoVI\text{-}B'}$/$Asn46^{GyrB}$, which radicicol does not contact. Moreover, whereas radicicol nestles almost entirely inside the ATP-binding pocket, large segments of novobiocin and GR122222X lie outside the pocket and contact residues that are not conserved across type II topoisomerases. For example, both novobiocin and GR122222X ligand Arg136 of GyrB, an amino acid that lies outside the

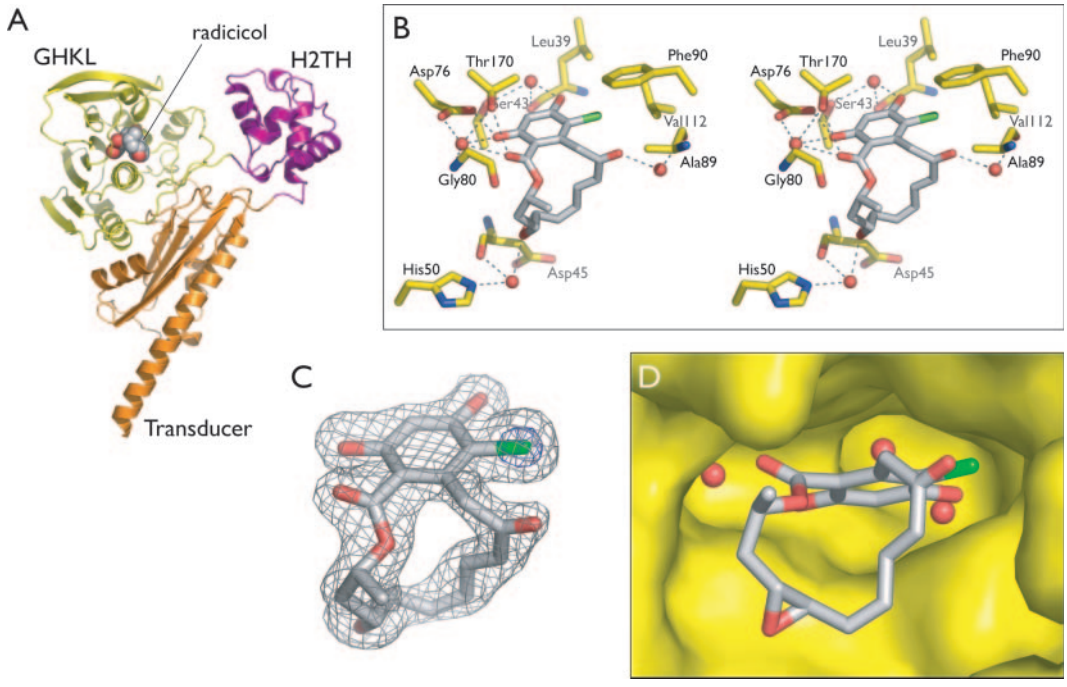

Figure 2. The structure of monomeric topoVI-B′ bound to radicicol. (**A**) Ribbon diagram of the topoVI-B′-radicicol complex. The GHKL domain is shown in yellow, the H2TH domain purple, and the transducer domain orange. Radicicol is shown as spheres, bound to the GHKL domain. (**B**) Stereo view of the interactions between radicicol and topoVI-B′. (**C**) Simulated-annealing omit $F_o - F_c$ difference density for radicicol bound to topoVI-B′. Density in gray is shown contoured at 2.5 σ, and in blue at 10 σ around the exocyclic chlorine atom. (**D**) A view of radicicol (sticks) and its coordinating water molecules (spheres) in its binding pocket in topoVI-B′ (yellow surface), highlighting the shape complementarily between the drug and protein.

Table 2. Comparison of radicicol interactions in topoVI-B′ and Hsp90

Radicicol atom	TopoVI-B′ interacting residue	Hsp90 interacting residue
Oxygen 1[a]	—	—
Oxygen 2	Thr170	—
	Asp76[b]	Asp79
Oxygen 3	(Gly80)[c]	(Gly83)
	(Thr170)	(Thr171)
Oxygen 4	(Leu39)	(Leu34)
	(Ser43)	
Oxygen 5	(Ala89)	—
Oxygen 6	(Asp45)	Lys44
	(His50)	
Chlorine 1	*Phe90*[d,e]	*Phe124*[d]
	Asn42	*Asn37*
	Val112	
Carbon 2	*Ile81*	*Met84*
Carbon 17	*Ile79*	*Ile82*
	TopoVI-B′-radicicol	Hsp90-radicicol
Buried protein surface area (Å^2)[f]	233	258
Surface complementarity (S_c)[f]	0.763	0.728

[a]Oxygen atoms are labeled by number in Figures 4C and D.
[b]Underlines indicate interactions shared between topoVI-B and Hsp90.
[c]Parentheses indicate water-mediated interactions.
[d]Italics indicate van der Waals interactions.
[e]The phenylalanine residues from the two proteins originate from different secondary structural elements.
[f]Buried surface area and surface complementarity were computed considering three buried water molecules (best seen in Figure 2D) in each complex as part of the ligand.

radicicol-binding pocket and is not conserved in either archaeal or eukaryotic enzymes. Additionally, inside the ATP-binding pocket, GR122222X interacts with Glu50 of GyrB, which is substituted with alanine in topoVI-B′. This residue may be partly responsible for the natural resistance of gyrase to radicicol (24), since the larger glutamate residue in GyrB appears positioned to occupy the space needed to accommodate radicicol. Thus, despite the similarities between these three drugs' binding sites, structural and chemical differences between type II topoisomerase subfamilies, largely in residues other than those that bind ATP, help explain particular binding specificities.

Comparison of radicicol binding to topoVI-B′ and Hsp90

The GHKL domains of topo VI and Hsp90 share only ~ 10–12% sequence identity. Unsurprisingly, the structures of their GHKL domains are likewise fairly divergent: 107 Cα atoms in core secondary structural elements can be closely aligned with an r.m.s.d. of 1.9 Å, but over the length of their GHKL domains, the Cα r.m.s.d. exceeds 6 Å [*Saccharomyces cerevisiae* Hsp90, PDB ID 1BGQ, Ref. (47)] (Figure 4A). Despite these differences, the majority of amino acids and ordered water molecules that interact with radicicol in Hsp90 are shared with topoVI-B′, and overlay almost exactly when the two structures are compared (Figure 4B and Table 2). The common liganding interactions include several water-mediated hydrogen bonds, a direct hydrogen bond to Asp76$^{topoVI\text{-}B'}$/Asp79^{Hsp90}, and a van der Waals contact with Phe90$^{topoVI\text{-}B'}$/Phe124^{Hsp90}. In the latter instance, it is interesting to note

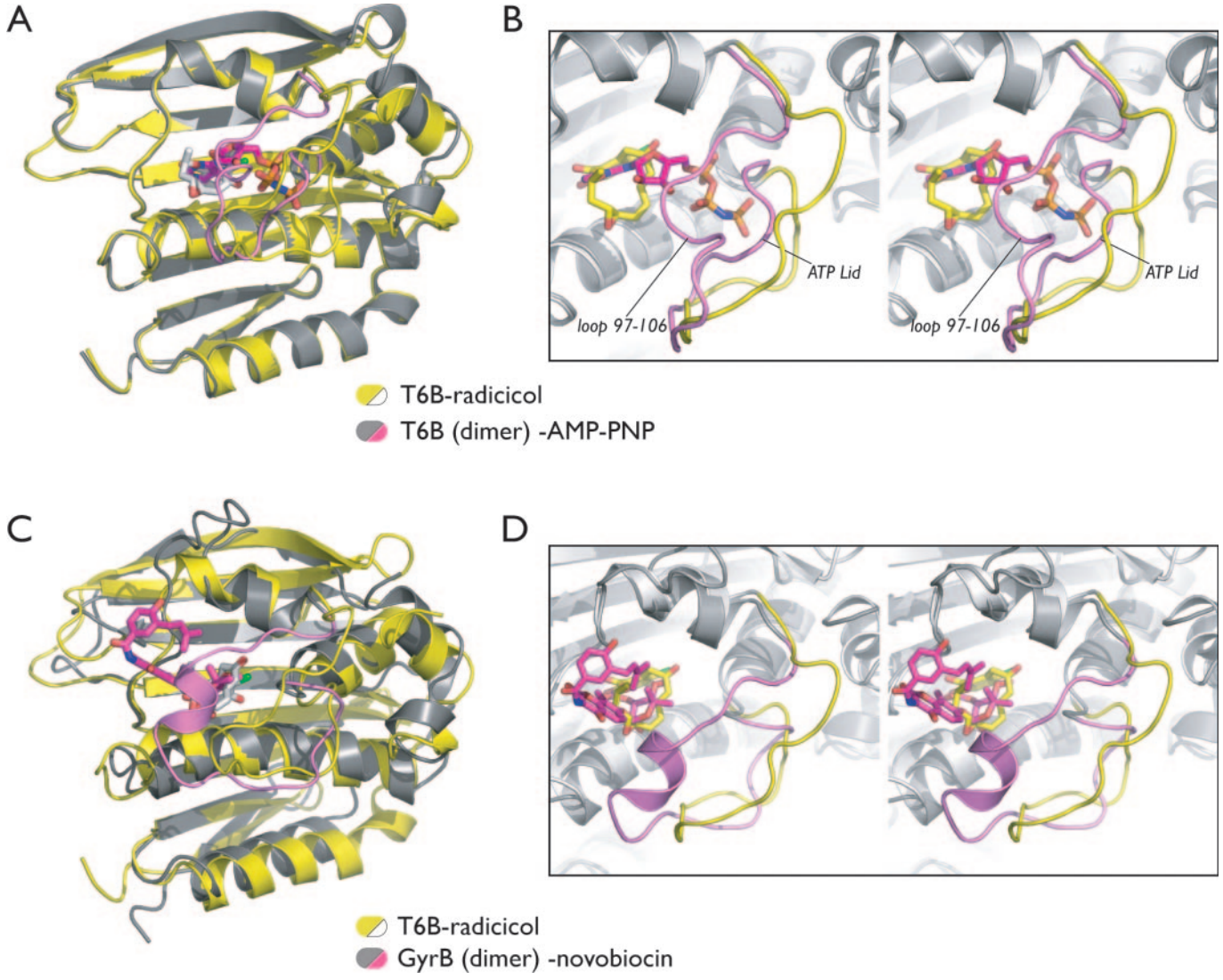

Figure 3. Comparison of radicicol, adenine nucleotide and coumarin drug binding to type II topoisomerases. (**A**) Structural overlay of the GHKL domains of radicicol-bound (yellow/white) and AMP-PNP-bound (gray/magenta) topoVI-B′ (17). (**B**) Close-up stereo view of the overlay shown in (A), with the ATP lid and adjacent loop residues 97–106 colored yellow (radicicol-bound) or magenta (AMP-PNP-bound, labeled). Radicicol competes for the same binding site as the adenine moiety of a nucleotide, but does not mediate protein conformational changes that allow dimerization. (**C**) Structural overlay of the GHKL domains of radicicol-bound topoVI-B′ (yellow/white) and the novobiocin-bound *Thermus thermophilus* GyrB dimer (gray/magenta) [Ref. (45), PDB code 1KIJ]. (**D**) Close-up stereo view of the overlay shown in (C). Both drugs bind in the ATPase site, but novobiocin additionally extends out of the active site to interact with residues specific to GyrB proteins. The ATP lid and adjacent loop in GyrB are rearranged to allow dimerization. Novobiocin makes several contacts with this region of GyrB (data not shown), but the interactions are not as extensive as those seen for bound nucleotide.

that these two phenylalanine residues occupy nearly the same space and form part of the hydrophobic 'ceiling' of the ATP-binding pocket, yet they actually originate from different secondary structural elements. Of the common radicicol-interacting residues, only one, $Asp76^{topoVI\text{-}B'}$/$Asp79^{Hsp90}$, is directly involved in nucleotide-binding; several others are involved in water-mediated interactions with nucleotide. The only major difference between the two proteins' interactions with radicicol lies outside the ATP-binding site, at the epoxide oxygen. Whereas topoVI-B′ interacts with this atom through two water-mediated hydrogen bonds (Figure 2B), Hsp90 ligands it directly through a lysine. Overall, the conservation between the radicicol-binding sites of Hsp90 and topoVI is remarkable, and explains why radicicol is able to bind these evolutionarily diverged enzymes.

It should be noted that despite the similarities between the two proteins' binding sites, radicicol inhibits the ATPase activity of *S.cerevisiae* Hsp90 at least 1000-fold more effectively than is seen for *S.shibatae* topoVI-B′ (47) (Figure 1A). The physical basis for this difference is not clear. The drug buries approximately the same amount of surface area when bound to either protein (Table 2). Respective surface complementarity (S_c) values for the two enzymes are highly similar as well, and there are no obvious steric clashes between topo VI and radicicol that might account for its reduced inhibition. One possibility is that the epoxide oxygen of radicicol, which associates directly with a lysine in Hsp90, but is liganded indirectly through a water-mediated hydrogen bond in topo VI, plays some role in tuning affinity. Alternatively, it is possible that the difference arises because of some

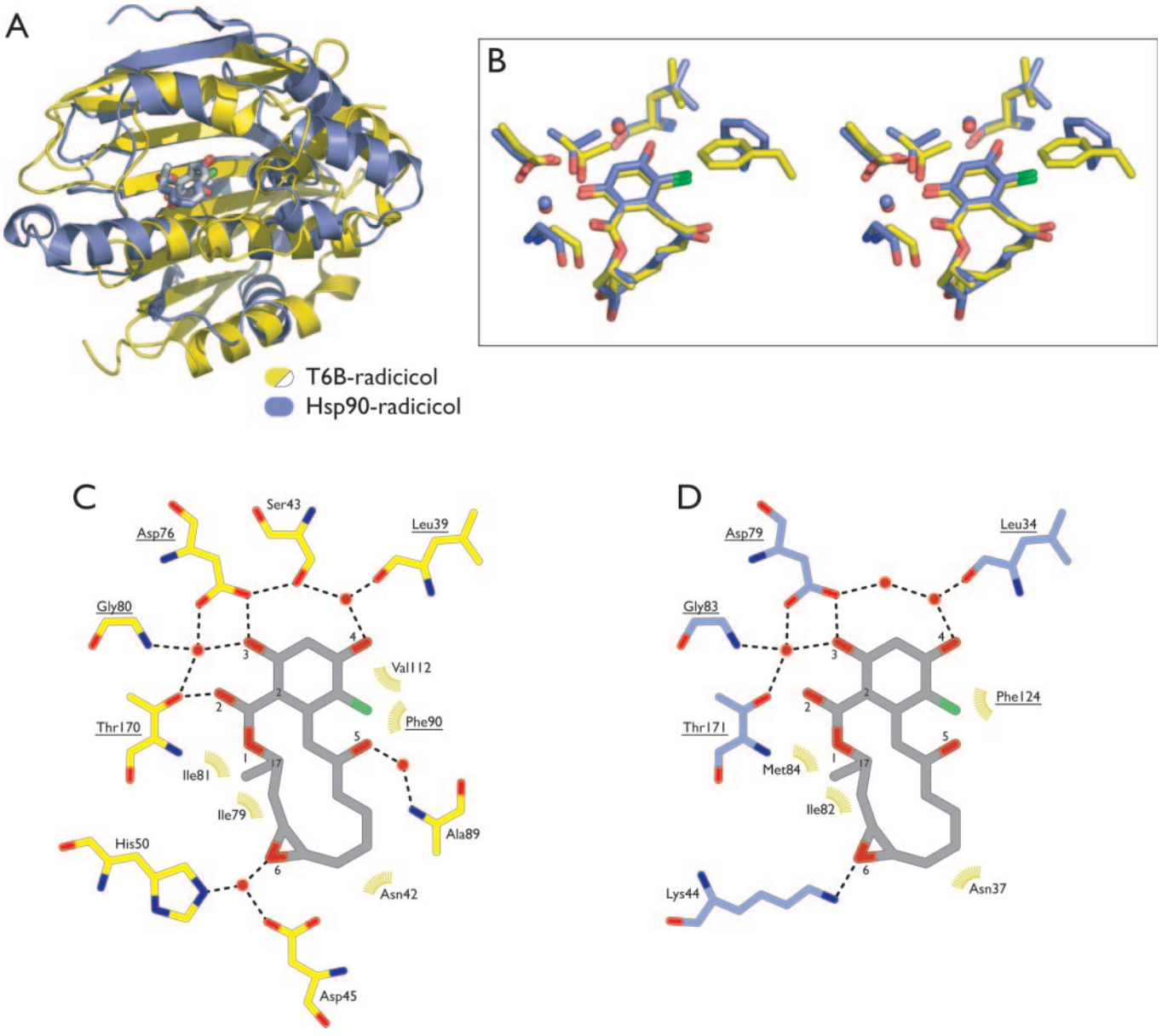

Figure 4. Comparison of radicicol binding to topoVI-B′ and Hsp90. (**A**) Structural overlay of radicicol-bound topoVI-B′ (yellow) and Hsp90 (blue) [Ref. (47), PDB code 1BGQ], superposed on the bound radicicol molecule. (**B**) Stereo view of an overlay between the active sites of topoVI-B′ (yellow with red waters) and Hsp90 (blue with blue waters) bound to radicicol, showing a shared constellation of interacting amino acids and liganding water molecules (drug binding residues not shared between the two enzymes are not shown in this panel). (**C** and **D**) Detailed views of the interactions of radicicol with topoVI-B′ (C) and Hsp90 (D). Drug-liganding amino acids that are conserved between the two proteins are underlined, and oxygen and select carbon atoms of radicicol are numbered.

necessary change in drug or protein structure that is slow to occur on the time scale of the activity assays (but resolved during the time required for crystallization), or that becomes manifest at the markedly different working temperatures for the two GHL proteins (30–37°C versus 65–80°C). Future mutagenesis and biochemical studies will be needed to explore this issue more thoroughly.

CONCLUSIONS

Our structural and biochemical results show that radicicol inhibits topo VI function by acting as a competitive inhibitor of ATP binding. Our findings also reveal that drug binding blocks dimerization of the ATPase domains, an event critical for T-segment capture and passage (Figure 5) (24). The ability of radicicol to specifically inhibit type IIB, but not type IIA topoisomerases could allow for its use *in vivo* to dissect the relative roles of type IIA and IIB topos in organisms that contain both enzyme classes. These include several bacterial species, certain archaea that contain a DNA gyrase evidently gained through horizontal gene transfer (48), and plants, where topo VI coexists with topo II and is required for a specialized genome amplification process known as endoreduplication (16,49,50). Radicicol may also be useful for exploring the molecular mechanisms of other GHL-family

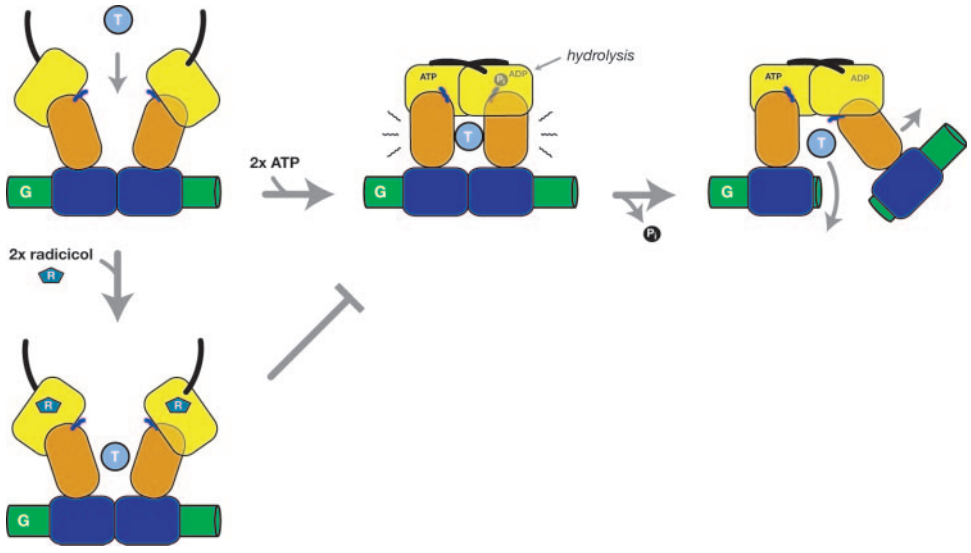

Figure 5. Functional consequences of radicicol on the reaction cycle of topoisomerase VI. The normal reaction cycle of topo VI begins when the T-segment (light blue) is trapped upon GHKL domain dimerization, an event facilitated by ATP binding. After ATP hydrolysis, the G-segment (green) is separated to allow T-segment passage. Radicicol can bind to the topoVI-B ATPase site to prevent ATP binding and GHKL domain dimerization, thus blocking T-segment capture and passage.

enzymes. For example, modeling suggests that the drug could fit comfortably in the ATP-binding pocket of MutL, and may bind topo II (data not shown).

Given the involvement of GHL enzymes in several critical cellular processes, from protein folding to DNA topology maintenance and repair, the design of new drugs to inhibit these enzymes is a high priority (43). The availability of a large set of structures showing GHL-family enzymes bound to different drugs reveals fascinating patterns of specificity combined with unexpected cross-reactivities. This situation likely arises from the interplay between two factors: a high degree of conservation within the ATP-binding site allows certain drugs to cross-react with very divergent enzymes, while structural differences outside this site concomitantly permit more specific targeting. With its small size and evident promiscuity in binding at least two highly diverged GHL-family enzymes, radicicol may prove an attractive scaffold on which to build more specific drugs that exploit unique structural features of other GHL family members.

ACKNOWLEDGEMENTS

The authors thank J. Holton, G. Meigs and J. Tanamachi for assistance at ALS Beamline 8.3.1 and D. S. Classen for helpful discussions. K.D.C. acknowledges support from a National Science Foundation pre-doctoral fellowship and J.M.B. acknowledges support from the NCI (CA077373). Funding to pay the Open Access publication charges for this article was provided by the NCI (CA077373).

Conflict of interest statement. None declared.

REFERENCES

1. Champoux,J.J. (2001) DNA topoisomerases: structure, function, and mechanism. *Ann. Rev. Biochem.*, **70**, 369–413.
2. Corbett,K.D. and Berger,J.M. (2004) Structure, molecular mechanisms, and evolutionary relationships in DNA topoisomerases. *Ann. Rev. Biophys. Biomol. Struct.*, **33**, 95–118.
3. Wang,J.C. (1998) Moving one DNA double helix through another by a type II DNA topoisomerase: the story of a simple molecular machine. *Q. Rev. Biophys.*, **31**, 107–144.
4. Wang,J.C. (2002) Cellular roles of topoisomerases: a molecular perspective. *Nature Rev. Mol. Cell. Biol.*, **3**, 430–440.
5. Andoh,T. and Ishida,R. (1998) Catalytic inhibitors of DNA topoisomerase II. *Biochim. Biophys. Acta*, **1400**, 155–171.
6. Burden,D.A. and Osheroff,N. (1998) Mechanism of action of eukaryotic topoisomerase II and drugs targeted to the enzyme. *Biochim. Biophys. Acta*, **1400**, 139–154.
7. Maxwell,A. (1999) DNA gyrase as a drug target. *Biochem. Soc. Trans.*, **27**, 48–53.
8. Roca,J. and Wang,J.C. (1994) DNA transport by a type II DNA topoisomerase: evidence in favor of a two-gate mechanism. *Cell*, **77**, 609–616.
9. Roca,J. and Wang,J.C. (1992) The capture of a DNA double helix by an ATP-dependent protein clamp: a key step in DNA transport by type II DNA topoisomerases. *Cell*, **71**, 833–840.
10. Wigley,D.B., Davies,G.J., Dodson,E.J., Maxwell,A. and Dodson,G. (1991) Crystal structure of an amino-terminal fragment of the DNA gyrase B protein. *Nature*, **351**, 624–629.
11. Corbett,K.D. and Berger,J.M. (2005) Structural dissection of ATP turnover in the prototypical GHL ATPase topo VI. *Structure*, **13**, 873–882.
12. Gellert,M., Mizuuchi,K., O'Dea,M.H. and Nash,H.A. (1976) DNA gyrase: an enzyme that introduces superhelical turns into DNA. *Proc. Natl Acad. Sci. USA*, **73**, 3872–3876.
13. Bergerat,A., Gadelle,D. and Forterre,P. (1994) Purification of a DNA topoisomerase II from the hyperthermophilic archaeon *Sulfolobus shibatae*: a thermostable enzyme with both bacterial and eucaryal features. *J. Biol. Chem.*, **269**, 27663–27669.
14. Bergerat,A., De Massy,B., Gadelle,D., Varoutas,P.-C., Nicolas,A. and Forterre,P. (1997) An atypical topoisomerase II from archaea with implications for meiotic recombination. *Nature*, **386**, 414–417.
15. Corbett,K.D. and Berger,J.M. (2003) Emerging roles for plant topoisomerase VI. *Chem. Biol.*, **10**, 107–111.
16. Hartung,F. and Puchta,H. (2001) Molecular characterization of homologues of both subunits A (SPO11) and B of the archaebacterial topoisomerase 6 in plants. *Gene*, **271**, 81–86.

17. Corbett,K.D. and Berger,J.M. (2003) Structure of the topoisomerase VI B subunit: implications for type II topoisomerase mechanism and evolution. *EMBO J.*, **22**, 151–163.
18. Diaz,R.L., Alcid,A.D., Berger,J.M. and Keeney,S. (2002) Identification of residues in yeast Spo11p critical for meiotic DNA double-strand break formation. *Mol. Cell. Biol.*, **22**, 1106–1115.
19. Nichols,M.D., DeAngelis,K., Keck,J.L. and Berger,J.M. (1999) Structure and function of an archaeal topoisomerase VI subunit with homology to the meiotic recombination factor Spo11. *EMBO J.*, **18**, 6177–6188.
20. Dutta,R. and Inouye,M. (2000) GHKL, an emergent ATPase/kinase superfamily. *Trends Biochem. Sci.*, **25**, 24–28.
21. Ban,C. and Yang,W. (1998) Crystal structure and ATPase activity of MutL: implications for DNA repair and mutagenesis. *Cell*, **95**, 541–552.
22. Ban,C., Junop,M. and Yang,W. (1999) Transformation of MutL by ATP binding and hydrolysis: a switch in DNA mismatch repair. *Cell*, **97**, 85–97.
23. Ali,M.M., Roe,S.M., Vaughan,C.K., Meyer,P., Panaretou,B., Piper,P.W., Prodromou,C. and Pearl,L.H. (2006) Crystal structure of an Hsp90-nucleotide-p23/Sba1 closed chaperone complex. *Nature*, **440**, 1013–1017.
24. Gadelle,D., Bocs,C., Graille,M. and Forterre,P. (2005) Inhibition of archaeal growth and DNA topoisomerase VI activities by the Hsp90 inhibitor radicicol. *Nucleic Acids Res.*, **33**, 2310–2317.
25. Lewis,R.J., Singh,O.M.P., Smith,C.V., Skarzynski,T., Maxwell,A., Wonacott,A.J. and Wigley,D.B. (1996) The nature of inhibition of DNA gyrase by the coumarins and the cyclothialidines revealed by X-ray crystallography. *EMBO J.*, **15**, 1412–1420.
26. Baykov,A.A., Evtushenko,O.A. and Avaeva,S.M. (1988) A malachite green procedure for orthophosphate determination and its use in alkaline phosphatase-based enzyme immunoassay. *Anal. Biochem.*, **171**, 266–270.
27. Lanzetta,P.A., Alvarez,L.J., Reinach,P.S. and Candia,O.A. (1979) An improved assay for nanomole amounts of inorganic phosphate. *Anal. Biochem.*, **100**, 95–97.
28. MacDowell,A.A., Celestre,R.S., Howells,M., McKinney,W., Krupnick,J., Cambie,D., Domning,E.E., Duarte,R.M., Kelez,N., Plate,D.W. *et al.* (2004) Suite of three protein crystallography beamlines with single superconducting bend magnet as the source. *J. Synchrotron Radiat.*, **11**, 447–455.
29. Holton,J. and Alber,T. (2004) Automated protein crystal structure determination using ELVES. *Proc. Natl Acad. Sci. USA*, **101**, 1537–1542.
30. Leslie,A.G.W. (1992) Recent changes to the MOSFLM package for processing film and image plate data. Joint CCP4 ESF-EAMCB newsletter on protein crystallography, No. 26. Daresbury Laboratories, Warrington, UK.
31. Storoni,L.C., McCoy,A.J. and Read,R.J. (2004) Likelihood-enhanced fast rotation functions. *Acta Crystallogr. D Biol. Crystallogr.*, **D60**, 432–438.
32. Murshudov,G.N., Vagin,A.A. and Dodson,E.J. (1997) Refinement of macromolecular structures by the maximum-likelihood method. *Acta Crystallogr. D Biol. Crystallogr.*, **53**, 240–255.
33. Lamzin,V.S. and Wilson,K.S. (1993) Automated refinement of protein models. *Acta Crystallogr. D Biol. Crystallogr.*, **49**, 129–147.
34. Winn,M.D., Isupov,M.N. and Murshudov,G.N. (2001) Use of TLS parameters to model anisotropic displacements in macromolecular refinement. *Acta Crystallogr. D Biol. Crystallogr.*, **57**, 122–133.
35. Brunger,A.T., Adams,P.D., Clore,G.M., DeLano,W.L., Gros,P., Grosse-Kunstleve,R.W., Jiang,J.S., Kuszewski,J., Nilges,M., Pannu,N.S. *et al.* (1998) Crystallography & NMR system: A new software suite for macromolecular structure determination. *Acta Crystallogr. D Biol. Crystallogr.*, **54**, 905–921.
36. Brunger,A.T., Adams,P.D. and Rice,L.M. (1997) New applications of simulated annealing in X-ray crystallography and solution NMR. *Structure*, **5**, 325–336.
37. Collaborative Computational Project, N. (1994) The CCP4 Suite: programs for protein crystallography. *Acta Crystallogr. D Biol. Crystallogr.*, **50**, 760–763.
38. Lawrence,M.C. and Colman,P.M. (1993) Shape complementarity at protein/protein interfaces. *J. Mol. Biol.*, **234**, 946–950.
39. DeLano,W.L. (2002) The PyMOL molecular graphics system. *DeLano Scientific,* San Carlos, CA.
40. Classen,D.S., Olland,S. and Berger,J.M. (2003) Structure of the topoisomerase II ATPase region and its mechanism of inhibition by the chemotherapeutic, ICRF-187. *Proc. Natl Acad. Sci. USA*, **100**, 10629–10634.
41. Roca,J., Ishida,R., Berger,J.M., Andoh,T. and Wang,J.C. (1994) Antitumor bisdioxopiperazines inhibit yeast DNA topoisomerase II by trapping the enzyme in the form of a closed protein clamp. *Proc. Natl Acad. Sci. USA*, **91**, 1781–1785.
42. Ali,J.A., Jackson,A.P., Howells,A.J. and Maxwell,A. (1993) The 43-kilodalton N-terminal fragment of the DNA gyrase B protein hydrolyzes ATP and binds coumarin drugs. *Biochemistry*, **32**, 2717–2724.
43. Maxwell,A. and Lawson,D.M. (2003) The ATP-binding site of type II topoisomerases as a target for antibacterial drugs. *Curr. Top. Med. Chem.*, **3**, 283–303.
44. Morris,S.K., Baird,C.L. and Lindsley,J.E. (2000) Steady-state and rapid kinetic analysis of topoisomerase II trapped as the closed-clamp intermediate by ICRF-193. *J. Biol. Chem.*, **275**, 2613–2618.
45. Lamour,V., Hoermann,L., Jeltsch,J.-M., Oudet,P. and Moras,D. (2002) An open conformation of the *Thermus thermophilus* gyrase B ATP-binding domain. *J. Biol. Chem.*, **277**, 18947–18953.
46. Tsai,F.T., Singh,O.M., Skarzynski,T., Wonacott,A.J., Weston,S., Tucker,A., Pauptit,R.A., Breeze,A.L., Poyser,J.P., O'Brien,R. *et al.* (1997) The high-resolution crystal structure of a 24-kDa gyrase B fragment from *E.coli* complexed with one of the most potent coumarin inhibitors, clorobiocin. *Proteins*, **28**, 41–52.
47. Roe,S.M., Prodromou,C., O'Brien,R., Ladbury,J.E., Piper,P.W. and Pearl,L.H. (1999) Structural basis for inhibition of the Hsp90 molecular chaperone by the antitumor antibiotics radicicol and geldanamycin. *J. Med. Chem.*, **42**, 260–266.
48. Gadelle,D., Filee,J., Buhler,C. and Forterre,P. (2003) Phylogenomics of type II DNA topoisomerases. *Bioessays*, **25**, 232–242.
49. Sugimoto-Shirasu,K., Stacey,N.J., Corsar,J., Roberts,K. and McCann,M.C. (2002) DNA topoisomerase VI is essential for endoreduplication in *Arabidopsis*. *Curr. Biol.*, **12**, 1782–1786.
50. Yin,Y., Cheong,H., Friedrichsen,D., Zhao,Y., Hu,J., Mora-Garcia,S. and Chory,J. (2002) A crucial role for the putative *Arabidopsis* topoisomerase VI in plant growth and development. *Proc. Natl Acad. Sci. USA*, **99**, 10191–10196.